In situ biomineralization of metal phytates in wood for improved bio-durability and flame retardancy

Aynun Nishat Farhabi
Graduate Research Assistant
Warnell School of Forestry and Natural Resources
University of Georgia, Athens, GA
Email: af14314@uga.edu

Liang Liang
Graduate Research Assistant
Department of Forest, Rangeland and Fire Sciences
University of Idaho, Moscow, ID
Email: lliang@uidaho.edu

Lili Cai *†
Associate Professor of Forest Biomaterials
Warnell School of Forestry and Natural Resources
University of Georgia, Athens, GA
Email: lcai@uga.edu

(Received 17 December 2025)

Abstract: This study investigated the in-situ biomineralization of metal phytate in wood to improve the antifungal and flame-retardant properties. Pine and aspen wood were impregnated with phytic acid and metal chlorides (copper, aluminum, and iron) via two treatment pathways. Path-1 involved treating wood with metal chlorides followed by phytic acid, while Path-2 involved the reverse order. Mass gain and accelerated leaching tests were performed to assess the treatment retention, followed by soil-block decay testing against four wood-decaying fungi and fire-related assessments on aspen via thermogravimetric analysis (TGA) and mass loss calorimeter (MLC) test. Path-2 resulted in significantly higher initial mass gain than Path-1, but experienced more substantial mass loss during leaching, indicating weaker fixation of PA-derived components. Before leaching, most treated samples exhibited improved decay resistance, with mass loss values below 10%. However, decay resistance decreased after leaching, indicating the importance of fixation stability for long-term durability. TGA showed that treated samples before leaching exhibited earlier thermal degradation and higher residual char yield than controls, while MLC measurements revealed reduced peak heat release rate, total heat release, and fire growth index, as well as higher char residue. Importantly, these flame-retardant properties were largely retained even after leaching. Overall, these results indicate that in situ metal–phytate formation can provide measurable improvements in fire performance, while fungal protection remains dependent on treatment retention. Further optimization of fixation chemistry is recommended to achieve more durable, bio-based wood protection.

Keywords: Metal phytate; Mineralization; Fungal resistance; Flame retardancy; Biobased wood protection.

Introduction

Wood is a widely available, renewable, and biodegradable construction material with excellent structural performance, favorable strength-to-weight ratio, and low environmental footprint (Zhu et al. 2016; Berglund and Burgert 2018; Jia et al. 2019). However, its hygroscopic nature and abundance of nutrient-rich polysaccharides make it highly susceptible to biological degradation by fungi (Råberg et al. 2005). Additionally, wood's inherent flammability limits its safe use in modern infrastructure without proper protective treatments. Therefore, enhancing both the bio-durability and fire resistance of wood remains critical for broadening its safe and sustainable applications.

Halogen-based flame retardants (chlorinated and brominated formulations) have historically been effective at improving fire resistance through radical-quenching mechanisms (Liang et al. 2013; Zhang et al. 2017). However, their combustion can generate toxic gases and persistent pollutants, raising serious health and environmental concerns (Venier et al. 2015; Kovačević et al. 2021; Ilyas et al. 2021). This has accelerated the shift toward halogen-free and bio-derived flame-retardant systems (Costes et al. 2017; Liang et al. 2023).

* Corresponding author
† Society of Wood Science & Technology member

Phytic acid (PA), a natural myo-inositol hexakisphosphate abundant in seeds and grains, contains six phosphate groups and exhibits high phosphorus content (~28 wt%) (Lott1 et al. 2000; Viveros et al. 2000; Loewus 2001; Costes et al. 2017; Gänzle 2020). PA is recognized as a promising bio-based, halogen-free flame retardant due to its strong dehydration and char-forming capability (Guo et al. 2019). PA also has strong metal-chelating ability, enabling the formation of metal phytates, which are thermally stable salts capable of improving char structure and reducing flammable volatiles (Kremer et al. 2020; Zhang et al. 2022). Prior studies demonstrate that PA or metal phytates can improve fire performance and even inhibit fungal growth in some cases (Wang et al. 2022; Liang et al. 2024).

The fire performance of wood products was further improved, especially when synergized with chitosan (Zhao et al. 2020; Yang and Zhang 2022), protein (Li et al. 2021), urea (Antoun et al. 2022), uracil (Zhang et al. 2021), silica (Chen et al. 2021; Lin et al. 2023), polyelectrolyte complexes (Soula et al. 2021) and other chemical formulations reported in recent studies (Zhao et al. 2020; Tang and Fu 2020; Zhou and Fu 2020; Song et al. 2022; Tian et al. 2023). For example, Zhang et al. (2022) reported that metal-phytate-treated wood exhibited substantial smoke-suppression and flame-inhibition effects, achieving a 44.8% reduction in total heat release (THR) and a 92.0% reduction in total smoke production (TSP) compared with untreated wood. In another investigation, Zhang et al. (2023) found that a modest ~13.5% weight gain of copper phytate on the cell wall led to a 74.2% decrease in fire growth index, 85.4% lower smoke production, and a 33.3% decline in CO generation. Furthermore, Fan et al. (2024) demonstrated that applying phytic acid and zinc phytate to delignified wood via vacuum-pressure impregnation significantly enhanced the flame retardancy of Chinese fir, reducing THR from 55.66 MJ/m² to 5.90 MJ/m² and rapidly forming a compact, carbonized barrier. These improvements have been attributed to the synergistic dual-charring role of phosphorus and metal species, combined with the catalytic graphitization promoted by multivalent metal ions.

However, current research has primarily focused on fire performance, while the bio-durability of metal-phytate-treated wood, especially after leaching, remains insufficiently explored. This knowledge gap is crucial because water solubility and fixability strongly affect long-term performance in real-world environments. Additionally, in-situ biomineralization of metal phytates within the wood matrix is particularly advantageous, as it is hypothesized to facilitate mineral formation within cell walls and lumens, rather than solely on the surface. This internal precipitation is expected to enhance the fixation of phosphorus-metal species, minimize leaching, and produce a compact char layer during combustion, unlike surface-applied coatings or post-impregnation treatments. Furthermore, the sequence of chemical application may influence how phytates form and distribute within the wood structure, potentially altering fixation efficiency and overall protective behavior. Nevertheless, this has not been systematically investigated.

Inspired by recent phytate-based studies and existing knowledge gaps, this study uses three different metallic salts, namely, copper chloride, aluminum chloride, and ferric chloride, along with phytic acid, to generate metal phytates in-situ within samples of loblolly pine (*Pinus taeda* L.) and bigtooth aspen (*Populus grandidentata*) sapwood through a simple two-step impregnation process. Two different treatment pathways were designed to mimic different orders of phytate formation in wood. Path-1 involved treating wood with metal chlorides followed by phytic acid, while Path-2 involved the reverse order. The chloride salts of Cu^{2+}, Al^{3+}, and Fe^{3+} were selected for their high-water solubility, pronounced Lewis acidity, and facile dissociation, representing both divalent and trivalent systems. These characteristics allow a systematic assessment of how cation charge density and coordination behavior influence in-situ precipitation and localization of metal-phytate complexes within the wood structure. Additionally, due to differences in ion charge and stereochemistry, the sequence of addition may influence where solid metal-phytate deposits within wood, thereby affecting the distribution, depth of the deposit, and fixation efficiency.

Previous metal phytate/wood studies have demonstrated that several different metal species can be incorporated into wood to achieve excellent flame retardancy and smoke suppression, often within a single wood substrate and a fixed impregnation sequence. In contrast, the present study systematically compares three PA-based metal systems, two formation pathways (metal-PA vs. PA-metal), and two wood species (a softwood, loblolly pine, and a hardwood, bigtooth aspen) within one experimental matrix, while simultaneously assessing the leaching properties, fungal durability, and fire-retardant performance. These features allow us to examine how metal valence, solution acidity, and reagent sequence collectively influence in-situ formation and fixation of metal phytate complexes in wood, as reflected by mass gain, accelerated leaching test, decay resistance test, thermal stability, and mass loss calorimeter (MLC) test results.

Materials and method

Materials

PA solution (PA, $C_6H_{18}O_{24}P_6$, ca. 50% in water, ca. 1.1 mol/L, TCI, MW 660.03 g/mol), and three metal chlorides (denoted as M-Cl), including copper (II) chloride dihydrate ($CuCl_2 \cdot 2H_2O$, 99%, MW 170.48 g/mol), aluminum chloride hexahydrate ($AlCl_3 \cdot 6H_2O$, 99%, MW 241.43 g/mol), and iron (III) chloride anhydrous ($FeCl_3$, 98%, MW 162.21 g/mol) were purchased from Thermo Fisher Scientific Company, LLC (Waltham, MA, USA). These chemicals were diluted with deionized (DI) water into a PA solution of 0.0758 M and M-Cl solutions of 0.5 M at room conditions. The pH of all the treatment solutions is shown in Table 1.

Two brown-rot fungi, *Gloeophyllum trabeum* (Madison 617/ATCC 11539; *G.t.*), and *Rhodonia placenta* (Fr.) (ATCC#11538, *R.p.*), and two white-rot fungi, *Trametes versicolor* (*Linnaeus: Fries*) *Lloyd*, (ATCC#42462, *T.v.*), and *Irpex lacteus* (*Fr.*) Fr. (ATCC#11245, *I.l.*) were obtained from ATCC and used in the decay test.

Sapwood of the softwood, loblolly pine (525 ± 32 kg/m^3), and the hardwood, bigtooth aspen (509 ± 9 kg/m^3), were cut into wafers measuring 18 mm × 18 mm × 5 mm (R × T × L) for fungal decay tests according to American Wood Protection Association (AWPA) standard E22-22 (AWPA 2022). Aspen blocks with dimensions of 100 mm × 100 mm × 10 mm (L × T × R) were further prepared for the fire performance test. All wood samples were conditioned at 60°C for 48 h or until constant weight was reached before treatment.

Wood samples treatments

The wood samples were treated with two treatment solutions, M-Cl solution (0.5 M) and PA solution (0.0758 M), sequentially or in the reverse order, which were referred to as Path-1 when the M-Cl solution was first impregnated and Path-2 when the PA solution was first impregnated, as shown in Table 1. For example, the wood samples that underwent treatment Path-1 were labeled as Cu-PA, Al-PA, and Fe-PA, depending on the metal chloride used. Similarly, the wood samples treated in Path-2 schemes were denoted as PA-Cu, PA-Al, and PA-Fe. Wood samples vacuum-impregnated with only DI water served as the control group.

The wood samples used for the durability test were sequentially vacuum-impregnated with the treatment solutions (PA and M-Cl, depending on the treatment path) at 10 kPa for 1 h. For the fire performance test, the aspen wood samples were first vacuum-impregnated with one of the treatment solutions at a pressure of 10 kPa for 1 h, followed by a pressure impregnation (827 kPa) with the second treatment solution for 30 min. Upon completion of the first treatment, the treated wood samples were thoroughly washed under a continuous flow of DI water, then carefully wiped before being subjected to the subsequent treatment. After the second treatment, wood samples were washed following the same process and were then conditioned at 60°C for 48 h, until they reached a constant mass, and the masses of the wood samples both before and after each phase of the treatment procedure were documented, and the mass gain of the wood samples was calculated by employing Equation [1] below:

Table 1. Wood samples treatment paths.

Treatment path	1st step	2nd step	Label	Label after leaching
Path-1	M-Cl salts	PA	M-PA	M-PA-L
Path-2	PA	M-Cl salts	PA-M	PA-M-L

Note: PA = phytic acid solution (0.0758 M, pH 0.92 ± 0.03). M-Cl denotes metal chloride solutions (0.5 M) prepared from $FeCl_3$, $AlCl_3 \cdot 6H_2O$, and $CuCl_2 \cdot 2H_2O$, with pH values of 1.12 ± 0.02, 2.30 ± 0.02, and 2.76 ± 0.02, respectively.

$$Mass\ gain_{treat}\ (\%) = \frac{M_T - M_{UT}}{M_{UT}} \times 100\ \% \qquad [1]$$

where M_{UT} and M_T represent the masses of oven-conditioned wood samples before and after chemical treatment, respectively. The mass gain calculation included 12 replicates per treatment group. A detailed after-treatment mass gain plot for all treatment groups is shown in Figure S1 (Appendix).

Accelerated leaching test

An accelerated leaching test was performed on half of the wood samples in each treatment group, following the guidelines of the AWPA E11-16 standard (AWPA 2022) with some modifications. Six replicates from each treatment group intended for the durability test were immersed separately in 80 ml of deionized water (wood-to-water volume ratio 1:8) in individual beakers and vacuum-impregnated for 30 min. Likewise, three replicates from each treatment group designated for the fire performance test were immersed separately in 1200 ml of DI water (wood-to-water volume ratio 1:4) and vacuum-impregnated for 30 min. After impregnation, the leachate was discarded and replaced with an equal volume of fresh DI water. The beakers containing the wood samples were then agitated at 100 rpm for 4 h at room temperature, after which the leachates were again replaced with fresh DI water. This process was repeated until a total of

nine leachates had been replaced. The wet mass of the wood samples and their conditioned mass after oven-drying at 60°C for 48 h were recorded to determine the mass gain after leaching using Equation [2]. Wood samples subjected to leaching under Path-1 were labeled Cu-PA-L, Al-PA-L, and Fe-PA-L, while those under Path-2 were denoted PA-Cu-L, PA-Al-L, and PA-Fe-L (Table 1). The control group before and after leaching was designated control and control-L, respectively.

$$Mass\ gain_{leach}\ (\%) = \frac{M_L - M_{UT}}{M_{UT}} \times 100\% \quad [2]$$

Where M_{UT} and M_L represent the masses of oven-conditioned wood samples before chemical treatment and after leaching, respectively.

Fungal decay test

The fungal resistance of the in-situ biomineralized phytate wood samples (both before and after leaching) was evaluated following the AWPA E22-22 standard (AWPA 2022), with a minor adjustment to the sterilization procedure, as mentioned by Alorbu et al. (2023). Briefly, all wood samples were surface-sterilized by spraying with 70% ethanol and air-dried in a biosafety hood for 90 min. Each treatment group was subjected to a test fungus in soil culture bottles, with six replicates per group. The culture bottles were then incubated in the dark at 25°C and 75% relative humidity for 4 weeks. After the exposure period, the mycelia from the decayed wood were carefully removed by gentle brushing. The wet mass of the decayed samples was recorded, followed by oven-conditioning at 60°C for 48 h (or until a constant mass was achieved) to obtain the post-exposure dry mass. The moisture content (MC) and mass loss of decayed wood samples were determined using the following two equations:

$$Moisture\ content\ (\%) = \frac{(M_{wet} - M_{expo.})}{M_{expo.}} \times 100 \quad [3]$$

$$Mass\ loss\ (\%) = \frac{(M_{UT} - M_{expo.})}{M_{UT}} \times 100 \quad [4]$$

where M_{UT} refers to the dry mass of wood samples after conditioning (at 60°C for 48 h) before fungal exposure, whereas M_{expo} refers to the dry mass of wood samples after conditioning (at 60°C for 48 h) following fungal exposure. M_{wet} denotes the wet mass of the samples after undergoing decay. The detailed MC data of all the samples after the fungal decay test are provided in Table S1 (Appendix).

Thermogravimetric analysis

The thermal degradation properties of control and treated aspen wood samples (before and after leaching) were analyzed using thermogravimetric analysis (TGA) on a PerkinElmer TGA-7 instrument (Shelton, CT) under nitrogen (N_2) and air atmospheres. The samples (about 5–6 mg under each treatment group) were heated from room temperature to 800°C at a rate of 20°C/min under a gas flow of 30 mL/min. Thermogravimetric (TG) and derivative thermogravimetric (DTG) curves were recorded under both nitrogen and air atmospheres. The onset degradation temperature was determined as the intersection of tangents drawn at the baseline and the steepest part of the primary mass-loss region. The maximum degradation rate and its corresponding temperature (peak DTG) were identified from the extrema of the DTG curve. Residual mass at 800°C under N_2 and air was considered the final char/ash yield. All values listed in Table 2 represent the mean ± standard deviation of three replicates per treatment group.

Mass loss calorimeter test

The fire performance tests on the Path-1 and Path-2 treated wood blocks were conducted using the MLC (Fire Testing Technology, United Kingdom). The tests were carried out at an irradiation of 50 kW/m^2, in accordance with the ISO 13927 standard. The peak heat release rate (pHRR), the heat release rate (HRR), the total heat release (THR), and the amount of mass loss were recorded and examined. The wood samples treated with DI water alone were included as the control group and evaluated alongside the other treated wood samples for comparison.

Statistical analysis

The mass gain, mass loss, TGA, and MLC data were analyzed using one-way analysis of variance (ANOVA) in SAS 9.4 (SAS Institute Inc., Cary, NC) and R version 3.6.3. All statistical tests were conducted at a 95% confidence level ($\alpha = 0.05$). When significant differences were detected, post hoc comparisons were performed using Tukey's pairwise test or the Games-Howell test, depending on the homogeneity of variance.

Results and discussion

Mass gain

Mass gain of wood samples after treatment and leaching tests is shown in Figure 1. The control samples treated with (DI) water exhibited negative mass gains (pine: −0.88%; aspen: −0.45%), which were significantly lower ($p < 0.05$) than those of all other treatment groups. Overall, irrespective of treatment

Table 2. Onset temperature and residue of control and treated samples before and after leaching after the TGA test.

	N_2			Air			
Treatment	Onset (°C)	Degradation rate at peak T (%/min)	Residue (%)	1st Onset (°C)	2nd Onset (°C)	Degradation rate at peak T (%/min)	Residue (%)
Control	344 ± 1^{ab}	-24.66 ± 0.06^{ab}	11 ± 1^{ef}	341 ± 1^{a}	469 ± 2^{efg}	-51.92 ± 2.05^{bcd}	0 ± 0^{f}
Control-L	351 ± 4^{a}	-25.72 ± 0.3^{ab}	8.1 ± 1^{g}	336 ± 1^{ab}	480 ± 2^{cde}	-51.23 ± 1.30^{bc}	0 ± 0^{f}
Cu-PA	307 ± 2^{h}	-32.69 ± 1.04^{cd}	17 ± 1^{ab}	304 ± 5^{gh}	507 ± 6^{a}	-50.85 ± 0.63^{b}	0.4 ± 1^{def}
Cu-PA-L	340 ± 1^{bcd}	-35.50 ± 0.7^{d}	11 ± 1^{fg}	324 ± 2^{cd}	490 ± 5^{bc}	-52.43 ± 1.03^{bcd}	0 ± 0^{f}
Al-PA	322 ± 1^{fg}	-23.38 ± 4.27^{b}	14 ± 1^{cdef}	316 ± 7^{def}	462 ± 6^{fgh}	-74.84 ± 0.94^{f}	2.2 ± 1^{bc}
Al-PA-L	342 ± 1^{abc}	-30.68 ± 0.87^{c}	11 ± 2^{fg}	329 ± 3^{bc}	475 ± 4^{def}	-57.62 ± 3.39^{cde}	1.2 ± 1^{cde}
Fe-PA	336 ± 1^{bcd}	-25.44 ± 0.93^{ab}	15 ± 1^{bcd}	309 ± 1^{fg}	438 ± 5^{ij}	-35.29 ± 1.06^{a}	1.6 ± 1^{bcd}
Fe-PA-L	337 ± 2^{bcd}	-32.04 ± 1.93^{cd}	12 ± 1^{def}	315 ± 1^{def}	486 ± 2^{bcd}	-49.04 ± 0.76^{b}	2 ± 1^{bc}
PA-Cu	314 ± 1^{gh}	-32.42 ± 1.29^{cd}	18 ± 1^{a}	298 ± 2^{hi}	430 ± 6^{j}	-37.51 ± 0.78^{a}	2.8 ± 1^{ab}
PA-Cu-L	322 ± 4^{fg}	-35.38 ± 1.74^{d}	14 ± 1^{cdef}	315 ± 1^{def}	451 ± 1^{hi}	-47.28 ± 2.01^{b}	0.3 ± 1^{ef}
PA-Al	323 ± 2^{efg}	-21.95 ± 1.13^{ab}	17 ± 1^{abc}	305 ± 3^{gh}	459 ± 2^{gh}	-61.00 ± 0.58^{e}	2.2 ± 1^{bc}
PA-Al-L	330 ± 3^{def}	-24.31 ± 0.98^{a}	13 ± 2^{def}	321 ± 1^{cde}	495 ± 1^{ab}	-61.92 ± 0.88^{e}	2 ± 1^{bc}
PA-Fe	333 ± 3^{cde}	-25.18 ± 1.01^{ab}	15 ± 1^{bcde}	289 ± 5^{i}	381 ± 13^{k}	-52.37 ± 4.49^{bcd}	3.8 ± 1^{a}
PA-Fe-L	336 ± 4^{bcd}	-34.64 ± 1.50^{d}	13 ± 1^{def}	312 ± 1^{efg}	472 ± 1^{defg}	-58.21 ± 4.53^{de}	2.1 ± 1^{bc}

type or pathway, pine samples exhibited mass gains that were significantly higher ($p < 0.05$) than for aspen samples. The only exception was the Fe-PA groups, in which pine (3.67%) and aspen (3.78%) showed no statistically significant differences ($p > 0.05$). The greater mass gain observed in pine may be attributed to the anatomical differences between softwood and hardwood, as previously noted (Ding et al. 2008).

When comparing the two treatment pathways, Path-2 consistently resulted in significantly higher mass gains ($p < 0.05$) than Path-1 for both pine and aspen. Specifically, pine samples treated under Path-1 and Path-2 showed mass gains of approximately 3.6%–4.5% and 6%–11%, respectively, while aspen samples showed mass gains of about 1%–4% and 4%–6%. Among all groups, the Path-2 PA-Al treatment produced the

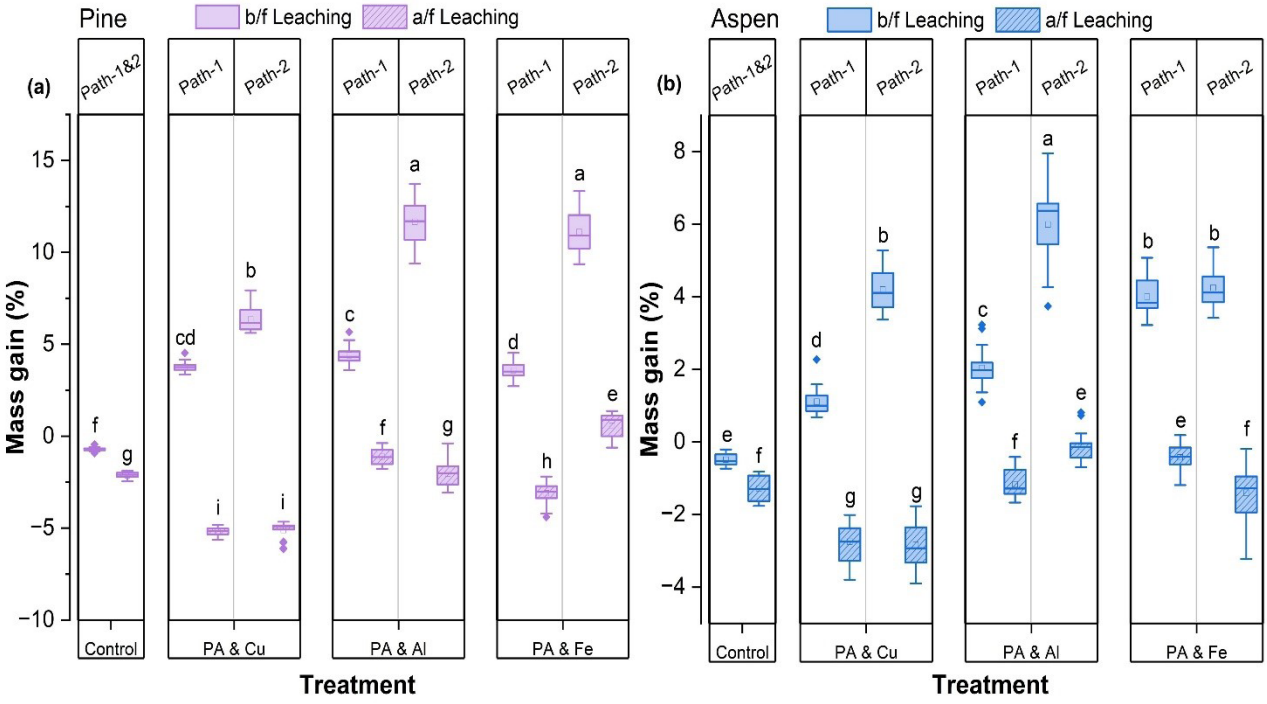

Figure 1. (a) Mass gain of pine samples before and after leaching test; (b) Mass gain of aspen samples before and after leaching test (n = 6).

highest mass gains, reaching 11.16% in pine and 6.12% in aspen (Figure 1).

However, after the accelerated leaching test, nearly all treatment groups (except PA-Fe-L in pine, 0.56%) showed significantly lower mass gains ($p < 0.05$) compared with their pre-leaching values (Figure 1a,b), regardless of wood species. Among the treatments, PA-Al and PA-Cu exhibited the greatest leaching losses, as indicated by the pronounced reductions in mass gain values. In contrast, the mass gains of Cu-PA-L and PA-Cu-L samples did not differ significantly after leaching ($p > 0.05$) for either pine or aspen. Overall, the leaching test revealed that Path-2 treatments were more prone to leaching than Path-1 treatments.

The possible reason could be that under Path-2, the introduction of metal ions into PA-saturated wood leads to rapid complexation and precipitation near the wood surface, forming surface-enriched metal-phytate deposits. This instantaneous reaction can partially block lumens and pits, physically retaining a larger amount of solids near the specimen surface and resulting in a higher apparent mass gain. In addition, incomplete conversion of PA during the second treatment step likely leaves a fraction of PA unreacted or weakly complexed, further contributing to mass gain. However, these surface-localized deposits and loosely bound PA species are more susceptible to removal upon water exposure, leading to greater leaching losses during the accelerated leaching test (Kremer et al. 2020; Marolt et al. 2020; Zhang et al. 2022). In contrast, under Path-1, metal cations are first able to diffuse into the wood structure and interact with negatively charged sites within the cell wall. Subsequent introduction of PA may promote in-situ precipitation at these pre-anchored locations, resulting in a more uniformly distributed and better-fixed metal-phytate network. Although this sequence may produce a lower initial mass gain, it likely enhances fixation efficiency and reduces leachability compared to Path-2 (Fan et al. 2024; Lebow 1996; Zhang et al. 2023).

Bio-durability test

Figure 2 shows the extent of mass loss in both control and treated wood samples (with and without leaching) after a 4-week exposure to the brown-rot (pine) and white-rot fungi (aspen). In general, control samples exposed to fungal attack showed an average mass loss ranging from 21%–34%. Similarly, the control-L group exhibited mass losses of 24%–38%, with no significant difference ($p > 0.05$) compared to the control. The substantial mass losses observed in the control groups can be attributed to the leaching of extractives throughout the decay exposure period (Sun et al. 2023).

In contrast, mycelial growth on treated samples was markedly inhibited, relative to the controls, regardless of leaching. Most treatment groups (both leached and unleached) exhibited mass losses below 10%, which were significantly lower than those of the controls ($p < 0.05$). However, exceptions were observed. The Al-PA group showed an average mass loss of 14% when exposed to *R.p.* ($p > 0.05$). In addition, Cu-PA-L, Al-PA-L, Fe-PA-L, PA-Cu-L, and PA-Al-L groups exposed to *R.p.*; the Al-PA-L and PA-Al-L groups exposed to *I.l.*; and the Al-PA-L group exposed to *T.v.* did not differ significantly from the control-L group. Moreover, PA-Al and PA-Cu treatment groups, which exhibited higher leachability and no significant difference in post-leaching mass gains, also showed relatively higher mass losses when exposed to *R.p*. Especially after leaching, Cu-PA-L, PA-Cu-L, and PA-Al-L groups recorded the highest mass losses under *R.p.* attack (Figure 2). These findings indicate that *R.p.* was the most aggressive fungus against the metal phytate treatments, while *G.t.* was the least aggressive among the four test fungi. In addition to mass loss, the moisture content of all samples after the 4-week exposure was determined to verify that conditions were suitable for fungal activity. The average MC of the control and control-L samples ranged from 28%–69% (Table S1, Appendix), which falls within or above the range generally considered favorable for brown-rot and white-rot decay (typically 30%–40% and often 40%–80%) (Lebow and Lebow 2018). Treated samples showed the average MC ranging from 27%–122% (Table S1, Appendix), which remained comparable or well above the minimum threshold for fungal growth, indicating that the lower mass loss in treated samples can be attributed to the efficacy of the metal-phytate treatment, rather than insufficient moisture.

Previous studies have also reported that inorganic metals, such as $FeCl_3$ and Al_2O_3, when fixed in treated wood, can enhance resistance against decay fungi (Acosta et al. 2022; Sun et al. 2023). Moreover, phytic acid has been reported to inhibit the growth of both brown-rot and white-rot fungi by limiting enzymatic activity (Li et al. 2023; Liang et al. 2024). The protective effect is further supported by the acidic nature of the phytate complexes (Table 1) that might have compromised the structural integrity of the fungal cell wall and diminished the activity of essential enzymes necessary for wood decay fungi. Collectively, these findings suggest that phytic acid-metal treatments confer substantial decay resistance, although susceptibility varies depending on both the fungal species and the leaching stability of the respective treatments.

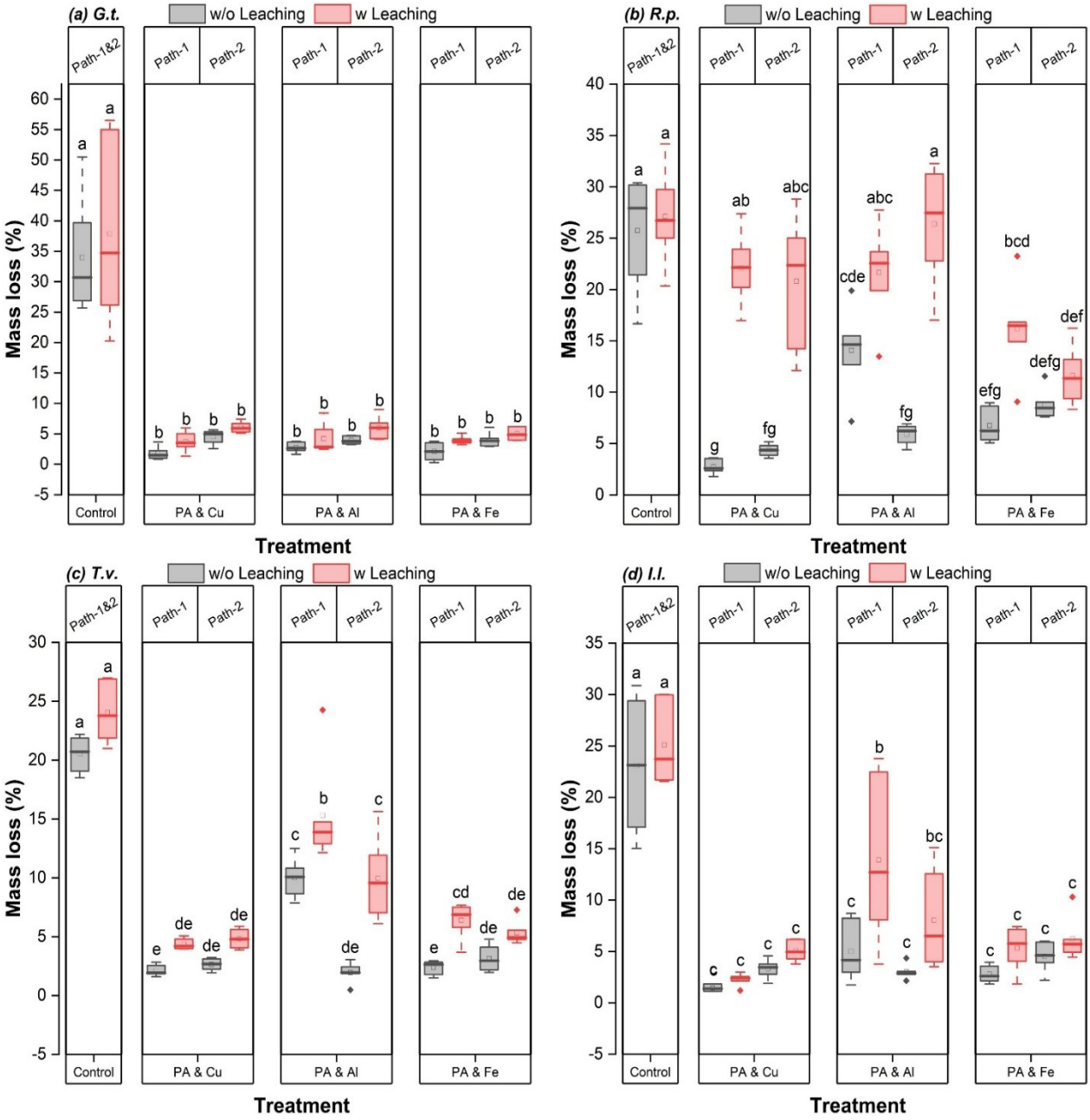

Figure 2. Mass loss of control and treated samples with and without leaching after exposure to each fungus: (a) *G.t.*; (b) *R.p.*; (c) *T.v.*; and (d) *I.l.* (n = 6).

Thermal stability

The thermal stability of the control and treated aspen wood samples was evaluated using thermogravimetric (TG) and derivative thermogravimetric (DTG) analyses under nitrogen (N_2) and air atmospheres (Figures 3 and 4), and the key parameters are summarized in Table 2.

Under N_2, the thermal decomposition of all samples followed three distinct stages, with a similar first stage but distinct temperature ranges for the second and third stages. Specifically, the first stage (30°C–160°C) involved the evaporation of moisture and light volatiles, corresponding to a minor mass loss (< 5%). For control and control-L samples, the mass of the samples remained relatively stable until reaching its second stage, from approximately 235°C to 550°C. This stage (a major weight loss of 80–85%) was mainly associated with the degradation of hemicellulose, cellulose, and lignin, with onset decomposition temperatures of 344°C for the control and 351°C for the control-L samples.

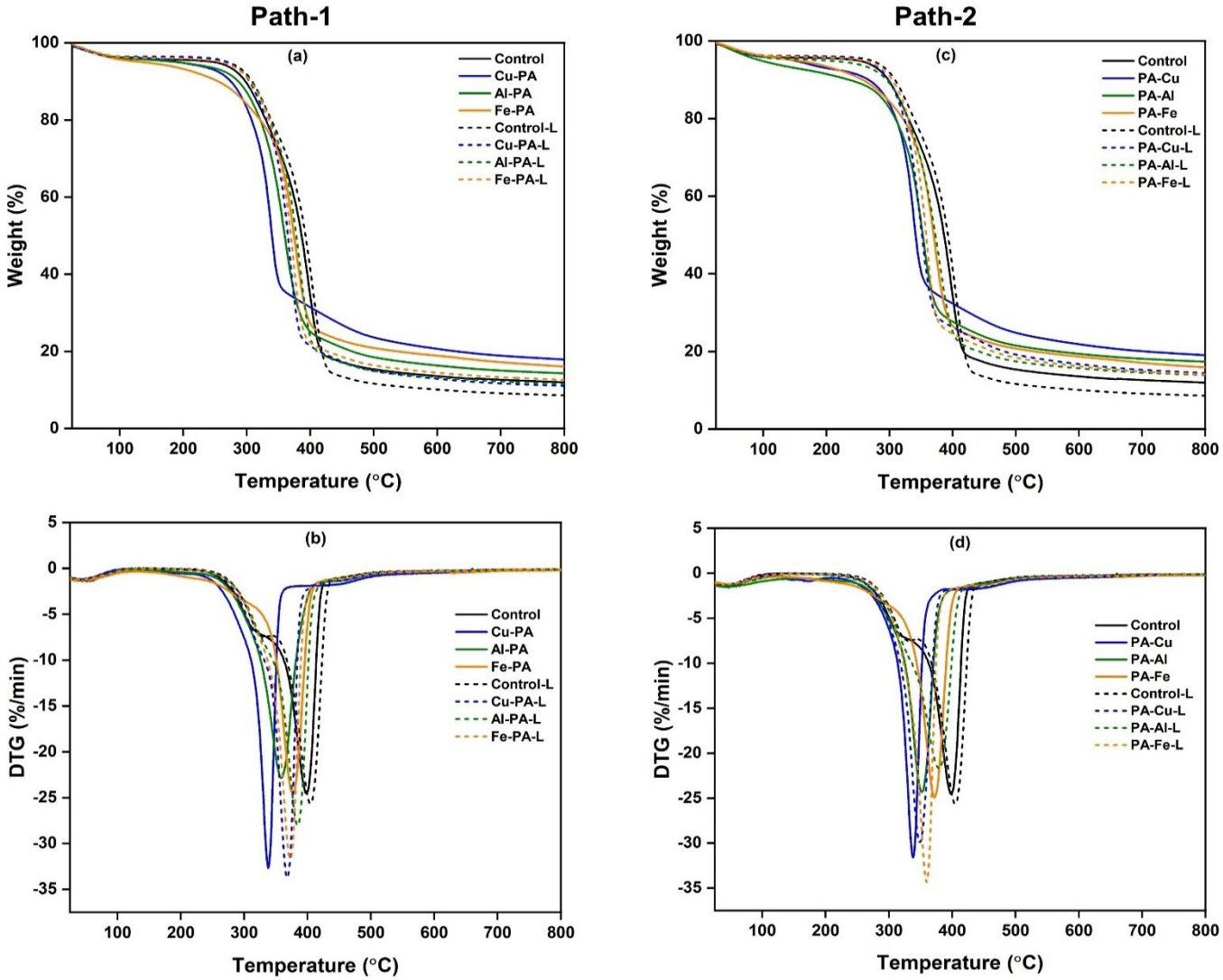

Figure 3. TG/DTG thermograms of control and treated samples before and after leaching (a, b) for Path-1; and (c, d) for Path-2 under N_2 (n = 3).

For the phytate-treated samples, the main decomposition shifted to lower temperatures of 180°C–450°C before leaching and 220°C–500°C after leaching, with onset temperatures of ~307°C–336°C and ~322°C–340°C, respectively. The corresponding mass losses were 64%–74% before leaching and 78%–82% after leaching. As shown in the DTG curves (Figure 3b,d), the peak decomposition temperatures of treated samples were 20°C–50°C lower than those of the controls (above 400°C), with the primary degradation peak appearing in the range of 300°C–400°C, indicating enhanced dehydration and char-promoting effects. This shift in the peak temperature of maximum degradation is attributed to the catalytic effect of the early decomposition of metal phytates, which accelerates char formation through phosphoric acid-induced dehydration reactions (Liu et al. 2022; Zhang et al. 2022). The third decomposition stage (450°C–800°C) corresponded to carbonization and aromatic char formation. All treated samples showed similar final-stage behavior, with total mass losses below 3%. The residual char yields of treated samples were significantly higher (14%–18% before leaching and 11%–14% after leaching) compared to the control (11%) and control-L (8%) samples, confirming improved thermal stability and non-volatile char retention.

The decomposition pattern under air followed a similar three-stage trend but included oxidative reactions in the later phase (Figure 4). During the first two stages, all samples exhibited comparable mass loss behavior up to ~315°C–365°C. However, control and control-L samples displayed an additional shoulder peak at 215°C–310°C, attributed to hemicellulose oxidation (Gao et al. 2004). This peak was absent in the phytate-treated

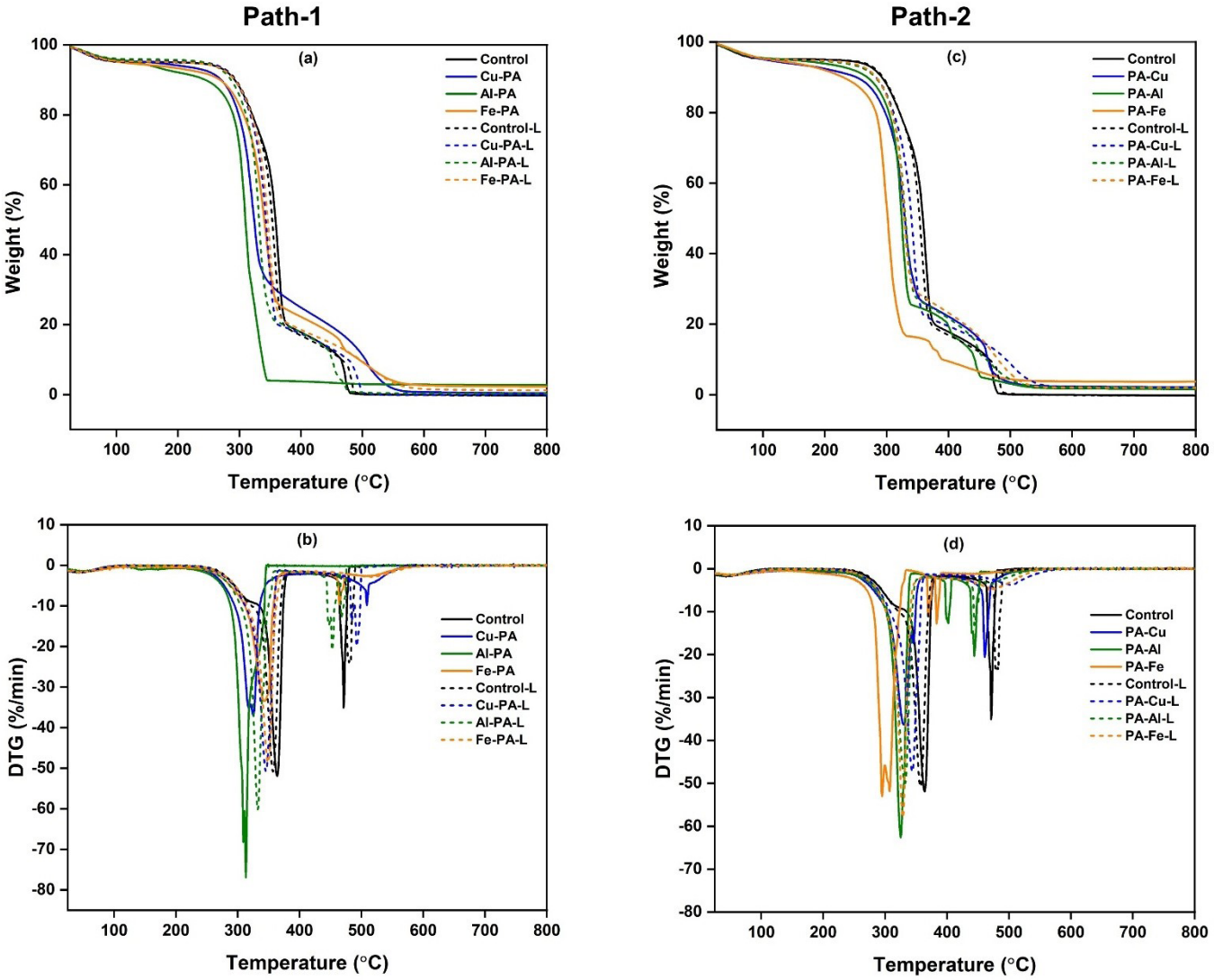

Figure 4. TG/DTG thermograms of control and treated samples before and after leaching (a, b) for Path-1; and (c, d) for Path-2 under Air (n = 3).

samples, indicating suppressed oxidative degradation due to the protective phosphorus-metal complex layer. In the third stage (> 400°C), the treated samples exhibited a narrower, delayed DTG peak (below 440°C) compared to controls, reflecting slower combustion of the carbonaceous char (Figure 4b,d). The primary degradation peak for all the treated samples (before and after leaching) appeared in the range of 300°C–350°C, whereas for the control samples, that degradation peak was observed above 380°C. Thus, the peak temperature at the peak thermal degradation rate of the treated samples was shifted towards a lower temperature range than the control and control-L, while their residual ash contents increased from 0% (control) to 0.4%–3.8% (treated), corresponding to the presence of thermally stable metal-phytate residues. These results demonstrate that metal-phytate formation effectively promotes early dehydration and crosslinking, while suppressing oxidative degradation at higher temperatures. The enhanced residue yield and reduced mass-loss rate confirm that the treated samples undergo a more controlled pyrolysis pathway, resulting in improved thermal stability and char integrity under both inert and oxidative environments.

Fire performance test

The MLC test was performed to assess the flame-retardant properties of the treated aspen wood samples. Figure 5 presents the heat release rate (HRR), total heat release (THR), and mass loss curves for control and treated wood samples before and after leaching, while Table 3 summarizes the key fire-performance parameters. Photographs of wood sample residues after combustion are shown in Figure 6.

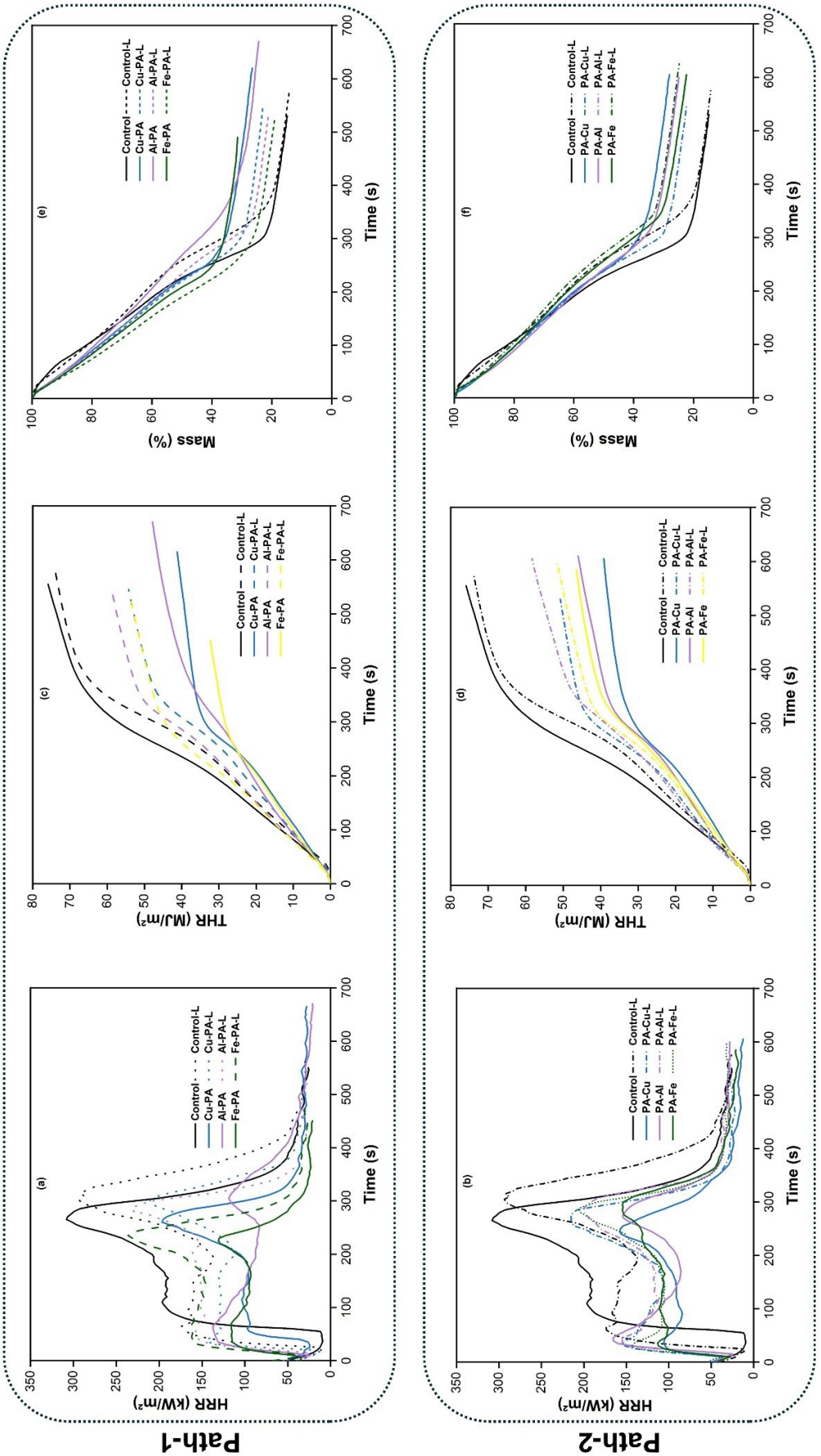

Figure 5. (a, b) Heat release rate (HRR); (c, d) total heat release (THR); and (e, f) mass loss curves of control and Path-1 and Path-2 treated samples before and after leaching following the mass loss calorimeter (MLC) test (n = 3).

Table 3. Mass loss calorimeter test data of all tested samples before and after the leaching test.

	Treatment	TTI (s)	TTF (s)	$pHRR_1$ ($k \cdot W/m^2$)	T_1 (s)	$pHRR_2$ ($k \cdot W/m^2$)	T_2 (s)	FGI ($k \cdot W/m^2.s^{-1}$)	THR ($M \cdot J/m^2$)	Residue (%)	Mass gain (%)
Path-1	Control	26±1^{a}	444±75^{abcd}	179±7^{a}	100±17^{a}	303±8^{a}	262±8^{bcd}	1.15±0.04^{a}	63±9^{ab}	15±2^{d}	-0.46±0.05^{f}
	Control-L	25±2^{a}	400±51^{bcd}	176±3^{ab}	73±11^{b}	284±14^{a}	298±11^{abc}	0.96±0.03^{bc}	65±4^{a}	14±1^{d}	-1.06±0.31^{f}
	Cu-PA	12±2^{bcd}	498±39^{ab}	104±7^{e}	50±13^{bc}	198±3^{bcd}	255±8^{cd}	0.78±0.04^{cd}	41±2de	26±0.70^{b}	11±0.20^{a}
	Cu-PA-L	14±3^{bc}	425±3^{abcd}	142±5^{bcd}	34±3^{c}	199±11^{bcd}	284±17^{abc}	0.70±0.02^{de}	46±3^{cd}	24±0.83^{bc}	0.02±0.99^{f}
	Al-PA	12±1^{bcd}	516±38^{a}	125±7de	55±5^{bc}	143±6^{e}	315±13^{a}	0.45±0.01^{f}	46±1^{cd}	24±1^{bc}	8.5±0.5^{b}
	Al-PA-L	14±2^{bcd}	406±4^{abcd}	162±3^{abc}	54±2^{bc}	225±8^{b}	288±10^{abc}	0.78±0.05^{cd}	53±1^{bc}	21±0.27^{c}	-0.85±0.42^{f}
	Fe-PA	12±1^{bcd}	347±22^{d}	98±18^{e}	53±11^{bc}	145±15^{e}	225±1^{d}	0.65±0.09^{de}	30±1^{e}	31±1^{a}	6.08±0.34^{cd}
	Fe-PA-L	13±1^{bcd}	376±24^{cd}	160±2^{abc}	44±3^{c}	217±19^{b}	230±10^{d}	0.96±0.05^{b}	49±4^{cd}	21±2^{bc}	-5.99±2^{h}
Path-2	PA-Cu	9±1^{d}	468±30^{abcd}	127±18de	34±3^{c}	164±13de	257±16^{cd}	0.64±0.07^{de}	40±3de	26±2^{bc}	8.04±0.50^{bc}
	PA-Cu-L	9±3^{d}	432±26^{abcd}	145±9^{bcd}	34±3^{c}	205±9^{bc}	275±10^{abc}	0.75±0.04^{de}	46±1^{cd}	23±1^{bc}	-3.66±0.56^{gh}
	PA-Al	12±2^{bcd}	485±5^{abc}	148±3^{abcd}	40±5^{c}	172±6^{cde}	282±3^{abc}	0.61±0.02^{ef}	44±3^{cd}	24±1^{bc}	5.05±0.33^{de}
	PA-Al-L	15±2^{b}	481±26^{abc}	152±7^{abcd}	42±3^{c}	185±13^{cd}	282±18^{abc}	0.66±0.06^{de}	52±2^{c}	24±2^{bc}	-1.76±0.19^{fg}
	PA-Fe	10±1^{cd}	490±56^{abc}	138±22^{cd}	38±17^{c}	175±21^{cde}	275±20^{abc}	0.64±0.10^{de}	46±3^{cd}	23±4^{bc}	3.67±1^{e}
	PA-Fe-L	13±1^{bcd}	482±19^{abcd}	143±6^{bcd}	35±5^{c}	200±9^{bcd}	302±17^{ab}	0.68±0.05^{de}	47±1^{cd}	26±0.84^{bc}	-1.47±0.53^{fg}

Note: pHRR refers to the highest HRR (Heat Release Rate) value; THR (Total heat Release) refers to the heat release calculated from the start of the test to 2 minutes after the flame out; Fire growth index, defined as the ratio of $pHRR_2$/ T_2.

Figure 6. Photographs of all tested samples before and after the mass loss calorimeter (MLC) test.

As shown in Figure 5a and 5b and in Table 3, the control and control-L samples exhibited rapid combustion, with HRR rising steeply and reaching early peak values ($pHRR_1$) of 179 kW/m² and 176 kW/m² at 100 s and 73 s, respectively. Prior to 250 s, intense pyrolysis and volatilization caused the surface layer of control samples to ignite quickly and transition into vigorous flaming, after which the surface began to char and form a carbonized layer (Guo et al. 2019). However, this char fractured as the burning duration increased, exposing deeper layers and leading to a second rise in HRR. This resulted in a secondary peak ($pHRR_2$) of 303 kW/m² and 279 kW/m² at 262 s and 298 s, respectively.

All treated samples, whether before or after leaching, exhibited markedly improved heat-release behavior. Although the time to $pHRR_1$ was advanced to 45–66 s (before leaching) and 19–39 s (after leaching) relative to the controls, the $pHRR_1$ values were reduced by 18%–45% before leaching and by 8%–29% after leaching. Similar improvements were observed for $pHRR_2$, with treated samples exhibiting reductions of 35%–53% before leaching and 19%–48% after leaching. Among all formulations, the Fe-PA treatment yielded the highest decrease in both peaks.

Figure 5c and 5d and Table 3 show that all treated samples released significantly less heat than the controls. The total heat released by treated samples was 27%–52% lower before leaching and 19%–29% lower after leaching than the control (63 MJ/m² for control, 65 MJ/m² for control-L). This reduction can be attributed to the formation of high-yield, thermally stable char layers derived from metal-phytate networks, which acted as physical barriers to heat and mass transfer. Similarly, the fire growth index (FGI)—the ratio of $pHRR_2$ to the time to peak—was consistently lower for treated samples than for controls, further indicating enhanced flame-retardant behavior. The Fe-PA sample again showed the strongest overall effect among the treatment groups.

As shown in Figure 5e and 5f and Table 3, irrespective of treatment pathways, the residual mass of all treated samples before and after leaching was significantly higher than the residual mass of the control (~15%) and control-L (~14%) samples. The residual mass values were recorded to be 54%–107% higher (for before-leaching samples) and 47%–80% higher (for after-leaching samples) compared to control and control-L samples, respectively. These findings are comparable to the existing literature, which reported that phosphorus-metal interactions promote dehydration, cross-linking, and graphitized carbon formation during combustion, resulting in more cohesive and thermally resistant char layers (Zhang et al. 2022, 2023). The time to ignition (TTI) of treated wood samples was 9–14 s, substantially lower than that of the control (~26 s) and control-L (~25 s). Similar reductions were reported for PA-treated wood by Liang et al. (2024), who attributed the shortened TTI to the acidic nature of PA. The acid promotes early dehydration and accelerates char formation, rather than allowing volatile, flammable gases to accumulate. Although the TTI was shorter, the overall heat release, peak intensity, and fire growth behavior were significantly reduced due to the protective char barrier.

After the MLC test (Figure 6), the control samples displayed fractured, brown-grey char. In contrast, all treated samples formed dense, cohesive, and continuous char layers that effectively shielded the underlying wood. Distinct coloration was also observed depending on the metal species. Under Path-1, Cu-PA samples produced bluish-black char, and Fe-PA samples yielded reddish-black char—corresponding to the known colors of $CuCl_2$ and $FeCl_3$ residues. Al-PA samples formed a whitish-black, highly stable char layer. These distinctive colors were less pronounced under Path-2, consistent with the shallower penetration and less uniform deposition of metal phytates.

Overall, the results indicate that metal-phytate complexes decompose at lower temperatures than wood polymers, releasing non-combustible products and promoting early char formation. The phosphorus-metal synergy facilitates dehydration, induces aromatic cross-linking, and enhances the graphitization of the carbonaceous residue (Zhang et al. 2022). This dual action restricts heat transfer and oxygen access, suppresses both primary and secondary combustion, and results in lower $pHRR_2$, THR, and FGI values, while increasing the final char yield. Even after leaching, the treated samples retained notable flame-retardant performance due to the persistent presence of phosphorus and metal species within the wood matrix.

Conclusions

This study examined the bio-durability and flame-retardant performance of wood treated through two sequential metal-phytate formation pathways. Overall, Path-2 resulted in higher initial mass gains, whereas Path-1 produced lower mass gains but generally better fixation and reduced leaching. After leaching, all treated samples exhibited lower retained mass, with Path-2 showing more pronounced loss, indicating limited long-term stability of loosely bound phytate species. The antifungal results demonstrated that most treated samples achieved improved decay resistance relative to the controls, although leached samples were less effective, and *R. placenta* remained the most aggressive fungus. Thermal and combus-

tion analyses indicated consistent enhancements in char formation and reduced heat-release behavior for all treatments. Thermogravimetric analysis showed an earlier onset of dehydration and higher char residue, while MLC testing confirmed reductions in $pHRR_2$ and THR and increases in residual mass, even after leaching. These results support that metal-phytate formation can promote catalytic charring and mitigate combustion intensity, although the magnitude of improvement varied among metals and pathways. Future work should focus on improving fixation chemistry, optimizing pH and reaction conditions, exploring crosslinking or buffering strategies, or incorporating co-treatments to stabilize PA-metal complexes.

Acknowledgements

This project was supported by the USDA NIFA Award #2022-67022-37607. Any opinions, findings, conclusions, or recommendations expressed in this publication are solely those of the authors and do not necessarily reflect the views of the U.S. Department of Agriculture. The authors would also like to thank Dr. Armando McDonald from the University of Idaho for access to FTIR and TGA.

References

Acosta AP, Gallio E, Cruz N, Aramburu AB, Lunkes N, Missio AL, Delucis R de A, Gatto DA (2022) Alumina as an antifungal agent for *Pinus elliottii* wood. J Fungi 8(12):1299. https://doi.org/10.3390/JOF8121299

Alorbu C, Carey J, McDonald AG, Cai L (2023) Antifungal properties of lauric arginate (LAE) treated wood. Holzforschung 77(8):640–647. https://doi.org/10.1515/HF-2023-0013/DOWNLOADASSET/SUPPL/J_HF-2023-0013_SUPPL_001.DOCX

Antoun K, Ayadi M, El Hage R, Nakhl M, Sonnier R, Gardiennet C, Le Moigne N, Besserer A, Brosse N (2022) Renewable phosphorous-based flame retardant for lignocellulosic fibers. Ind Crops Prod 186. https://doi.org/10.1016/j.indcrop.2022.115265

AWPA-American Wood Protection Association (2022) E22-22: Laboratory Method for Rapidly Evaluating the Decay Resistance of Wood-Based Materials Against Pure Basidiomycete Cultures Using Compression Strength: Soil/Wafer Test. AWPA Book of Standards, American Wood Protection Association, Birmingham, AL. 8 p. https://standards.globalspec.com/std/14519046/e22

AWPA-American Wood Protection Association (2022) E11-16 (2016, Reaffirmed 2022): Standard Method for Accelerated Evaluation of Preservative Leaching. AWPA Book of Standards, American Wood Protection Association, Birmingham, AL. 3 p. https://standards.globalspec.com/std/10030239/awpa-e11

Berglund LA, Burgert I (2018) Bioinspired wood nanotechnology for functional materials. Adv Mater 30(19):1704285. https://doi.org/10.1002/ADMA.201704285

Chen Z, Zhang S, Ding M, Wang M, Xu X (2021) Construction of a phytic acid-silica system in wood for highly efficient flame retardancy and smoke suppression. Materials 14(15):4164. https://doi.org/10.3390/MA14154164/S1

Costes L, Laoutid F, Brohez S, Dubois P (2017) Bio-based flame retardants: When nature meets fire protection. Materi Sci Eng R Rep 117:1–25. https://doi.org/10.1016/J.MSER.2017.04.001

Ding WD, Koubaa A, Chaala A, Belem T, Krause C (2008) Relationship between wood porosity, wood density and methyl methacrylate impregnation rate. Wood Mater Sci Eng 3(1–2):62–70. https://doi.org/10.1080/17480270802607947

Fan S, Gao X, Yang X, Li X (2024) Infusing phytate-based biomass flame retardants into the cellulose lumens of Chinese fir wood attains superior flame retardant efficacy. Int J Biol Macromol 258:128975. https://doi.org/10.1016/J.IJBIOMAC.2023.128975

Gänzle MG (2020) Food fermentations for improved digestibility of plant foods – an essential ex situ digestion step in agricultural societies? Curr Opin Food Sci 32:124–132. https://doi.org/10.1016/J.COFS.2020.04.002

Gao M, Shuying LI, Sun C (2004) Thermal degradation of wood in air and nitrogen treated with basic nitrogen compounds and phosphoric acid. Combust Sci Technol 176(12):2057–2070. https://doi.org/10.1080/00102200490514840

Guo H, Luković M, Mendoza M, Schlepütz CM, Griffa M, Xu B, Gaan S, Herrmann H, Burgert I (2019) Bioinspired struvite mineralization for fire-resistant wood. ACS Appl Mater Interfaces 11(5):5427–5434. https://doi.org/10.1021/ACSAMI.8B19967/ASSET/IMAGES/MEDIUM/AM-2018-199674_M002.GIF

Ilyas RA, Sapuan SM, Asyraf MRM, Dayana DAZN, Amelia JJN, Rani MSA, Norrrahim MNF, Nurazzi NM, Aisyah HA, Sharma S, Ishak MR, Rafidah M, Razman MR, Ilyas RA, Sapuan SM, Asyraf MRM, Dayana DAZN, Amelia JJN, Rani MSA, Norrrahim MNF, Nurazzi NM, Aisyah HA, Sharma S, Ishak MR, Rafidah M, Razman MR (2021) Polymer composites filled with metal derivatives: A review of flame retardants. Polymers 13(11):1701. https://doi.org/10.3390/POLYM13111701

Jia C, Chen C, Mi R, Li T, Dai J, Yang Z, Pei Y, He S, Bian H, Jang SH, Zhu JY, Yang B, Hu L (2019) Clear wood toward high-performance building materials. ACS Nano 13(9):9993–10001. https://doi.org/10.1021/acsnano.9b00089

Kovačević Z, Grgac SF, Bischof S, Kovačević Z, Grgac SF, Bischof S (2021) Progress in biodegradable flame retardant nano-biocomposites. Polymers 13(5):1–30. https://doi.org/10.3390/polym13050741

Kremer C, Torres J, Bianchi A, Savastano M, Bazzicalupi C (2020) Myo-inositol hexakisphosphate: Coordinative versatility of a natural product. Coord Chem Rev 419:213403. https://doi.org/10.1016/J.CCR.2020.213403

Lebow S (1996) Leaching of wood preservative components and their mobility in the environment—Summary of pertinent literature. Gen Tech Rep FPL-GTR-93. USDA Forest Service, Forest Products Laboratory, Madison, WI. 36 p. https://doi.org/10.2737/FPL-GTR-93

Lebow ST, Lebow PK (2018) Internal moisture content and temperature of standardized aboveground wood durability test specimens. Research Paper FPL-RP-694. USDA Forest Service, Forest Products Laboratory, Madison, WI. 14 p. https://doi.org/10.2737/FPL-RP-694

Li L, Chen Z, Lu J, Wei M, Huang Y, Jiang P (2021) Combustion behavior and thermal degradation properties of wood impregnated with intumescent biomass flame retardants: phytic acid, hydrolyzed collagen, and glycerol. ACS Omega 6(5):3921–3930. https://doi.org/10.1021/acsomega.0c05778

Li N, Wu YX, Zhang Y Di, Wang SR, Zhang GC, Yang J (2023) Phytic acid is a new substitutable plant-derived antifungal agent for the seedling blight of *Pinus sylvestris* var. *mongolica* caused by *Fusarium oxysporum*. Pestic Biochem Physiol 191:105341. https://doi.org/10.1016/J.PESTBP.2023.105341

Liang L, Alorbu C, McDonald A, Cai L (2024) Phytic acid for dual wood protection against fungi and fire. Wood Fiber Sci 56(2):72–82. https://doi.org/10.22382/wfs-2024-07

Liang S, Neisius NM, Gaan S (2013) Recent developments in flame retardant polymeric coatings. Prog Org Coat 76(11):1642–1665. https://doi.org/10.1016/J.PORGCOAT.2013.07.014

Liang Y, Jian H, Deng C, Xu J, Liu Y, Park H, Wen M, Sun Y (2023) Research and application of biomass-based wood flame retardants: A review. Polymers 15(4):950. https://doi.org/10.3390/polym15040950

Lin CF, Zhang C, Karlsson O, Martinka J, Mantanis GI, Rantuch P, Jones D, Sandberg D (2023) Phytic acid-silica system for imparting fire retar-

dancy in wood composites. Forests 14(5):1021. https://doi.org/10.3390/f14051021

Liu L, Zhu M, Ma Z, Xu X, Mohesen Seraji S, Yu B, Sun Z, Wang H, Song P (2022) A reactive copper-organophosphate-MXene heterostructure enabled antibacterial, self-extinguishing and mechanically robust polymer nanocomposites. Chem Eng J 430:132712. https://doi.org/10.1016/J.CEJ.2021.132712

Loewus FA (2001) Biosynthesis of phytate in food grains and seeds. Pp 53–62 in Reddy NR, Sathe SK, eds. Food Phytates. CRC Press, Boca Raton, FL. https://doi.org/10.1201/9781420014419.CH4

Lott1 JNA, Ockenden I, Raboy V, Batten GD (2000) Phytic acid and phosphorus in crop seeds and fruits: a global estimate. Seed Sci Res 10(1):11–33. https://doi.org/10.1017/S0960258500000039

Marolt G, Gričar E, Pihlar B, Kolar M (2020) Complex formation of phytic acid with selected monovalent and divalent metals. Front Chem 8:582746. https://doi.org/10.3389/FCHEM.2020.582746

Råberg U, Edlund ML, Terziev N, Land CJ (2005) Testing and evaluation of natural durability of wood in above ground conditions in Europe - An overview. J Wood Sci 51(5):429–440. https://doi.org/10.1007/S10086-005-0717-8

Song F, Liu T, Fan Q, Li D, Ou R, Liu Z, Wang Q (2022) Sustainable, high-performance, flame-retardant waterborne wood coatings via phytic acid based green curing agent for melamine-urea-formaldehyde resin. Prog Org Coat 162:106597. https://doi.org/10.1016/j.porgcoat.2021.106597

Soula M, Samyn F, Duquesne S, Landry V (2021) Innovative polyelectrolyte treatment to flame-retard wood. Polymers (Basel) 13(17):2884. https://doi.org/10.3390/polym13172884

Sun M, Zhao C, Alorbu C, Cai L, Yu Y, Sun M, Zhao C, Alorbu C, Cai L, Yu Y (2023) Antique wood preparation by inorganic salts treatment and its performance. Maderas ciencia y tecnología 25. https://doi.org/10.4067/S0718-221X2023000100423

Tang T, Fu Y (2020) Formation of chitosan/sodium phytate/nano-Fe_3O_4 magnetic coatings on wood surfaces via layer-by-layer self-assembly. Coatings 10(1):51. https://doi.org/10.3390/coatings10010051

Tian Y, Wang C, Ai Y, Tang L, Cao K (2023) Phytate-based transparent and waterproof intumescent flame-retardant coating for protection of wood. Mater Chem Phys 294:127000. https://doi.org/10.1016/j.matchemphys.2022.127000

Venier M, Salamova A, Hites RA (2015) Halogenated flame retardants in the Great Lakes environment. Acc Chem Res 48(7):1853–1861. https://doi.org/10.1021/ACS.ACCOUNTS.5B00180

Viveros A, Centeno C, Brenes A, Canales R, Lozano A (2000) Phytase and acid phosphatase activities in plant feedstuffs. J Agric Food Chem 48(9):4009–4013. https://doi.org/10.1021/jf991126m

Wang K, Meng D, Wang S, Sun J, Li H, Gu X, Zhang S (2022) Impregnation of phytic acid into the delignified wood to realize excellent flame retardant. Ind Crops Prod 176:114364. https://doi.org/10.1016/j.indcrop.2021.114364

Yang G, Zhang Q (2022) In situ polymerization and flame retardant mechanism of bio-based nitrogen and phosphorus macromolecular flame retardant in plywood. Macromol Rapid Commun 43(8):2200018. https://doi.org/10.1002/MARC.202200018

Zhang J, Wu Q, Li G, Li MC, Sun X, Ring D (2017) Synergistic influence of halogenated flame retardants and nanoclay on flame performance of high density polyethylene and wood flour composites. RSC Adv 7(40):24895–24902. https://doi.org/10.1039/C7RA03327C

Zhang L, Yi D, Hao J, Gao M (2021) One-step treated wood by using natural source phytic acid and uracil for enhanced mechanical properties and flame retardancy. Polym Adv Technol 32(3):1176–1186. https://doi.org/10.1002/pat.5165

Zhang S, Wang X, Ding M, Huang Y, Li L, Wang M (2022) In-situ incorporation of metal phytates for green and highly efficient flame-retardant wood with excellent smoke-suppression property. Ind Crops Prod 187:115287. https://doi.org/10.1016/j.indcrop.2022.115287

Zhang S, Zhao X, Peng Y, Yang T, Huang Y, Li L, Wang M (2023) In-situ synthesis of copper phytate-hierarchically porous MOF-199 hybrid in wood towards multifunctional flame-retardant wood composite. Ind Crops Prod 204:117233. https://doi.org/10.1016/J.INDCROP.2023.117233

Zhao F, Tang T, Hou S, Fu Y (2020) Preparation and synergistic effect of chitosan/sodium Phytate/MgO nanoparticle fire-retardant coatings on wood substrate through layer-by-layer self-assembly. Coatings 10(9):848. https://doi.org/10.3390/coatings10090848

Zhou L, Fu Y (2020) Flame-Retardant wood composites based on immobilizing with chitosan/sodium phytate/Nano-TiO2-ZnO coatings via layer-by-layer self-assembly. Coatings 10(3):296. https://doi.org/10.3390/coatings10030296

Zhu M, Song J, Li T, Gong A, Wang Y, Dai J, Yao Y, Luo W, Henderson D, Hu L, Zhu M, Song J, Li T, Gong A, Wang Y, Dai J, Yao Y, Luo W, Henderson D, Hu L (2016) Highly anisotropic, highly transparent wood composites. Adv Mater 28(26):5181–5187. https://doi.org/10.1002/ADMA.201600427

Appendix

Table S1. Average moisture content of the samples after decay (n = 6).

	Average moisture content (%) after decay			
Treatment	*G.t*	*R.p*	*T.v*	*I.l*
Control	45.77 ± 22.48	34.15 ± 4.48	58.82 ± 15.78	28.60 ± 6.49
Control-L	69.02 ± 31.66	41.02 ± 4.44	53.90 ± 7.78	31.47 ± 5.52
Cu-PA	69.02 ± 6.81	74.01 ± 17.47	46.42 ± 9.81	40.57 ± 10.43
Cu-PA-L	29.34 ± 6.27	37.44 ± 4.25	31.83 ± 3.59	28.10 ± 1.84
Al-PA	39.70 ± 11.75	33.57 ± 6.61	31.13 ± 9.05	35.26 ± 9.16
Al-PA-L	32.20 ± 11.92	37.67 ± 4.48	47.92 ± 14.60	34.19 ± 7.71
Fe-PA	49.50 ± 19.38	78.51 ± 16.64	43.99 ± 8.92	48.23 ± 12.18
Fe-PA-L	28.00 ± 2.67	68.09 ± 43.85	38.97 ± 3.80	40.61 ± 3.44
PA-Cu	88.27 ± 11.30	122.17 ± 10.85	97.63 ± 22.00	71.34 ± 2.02
PA-Cu-L	35.73 ± 11.56	41.72 ± 8.10	31.52 ± 3.58	33.32 ± 2.60
PA-Al	73.37 ± 11.91	97.67 ± 21.69	62.70 ± 4.20	88.47 ± 13.80
PA-Al-L	36.04 ± 12.10	43.01 ± 4.60	41.71 ± 8.15	43.97 ± 7.91
PA-Fe	60.71 ± 8.71	76.84 ± 14.14	57.45 ± 15.86	54.15 ± 15.70
PA-Fe-L	27.09 ± 2.74	36.49 ± 3.91	40.68 ± 9.47	47.49 ± 2.47

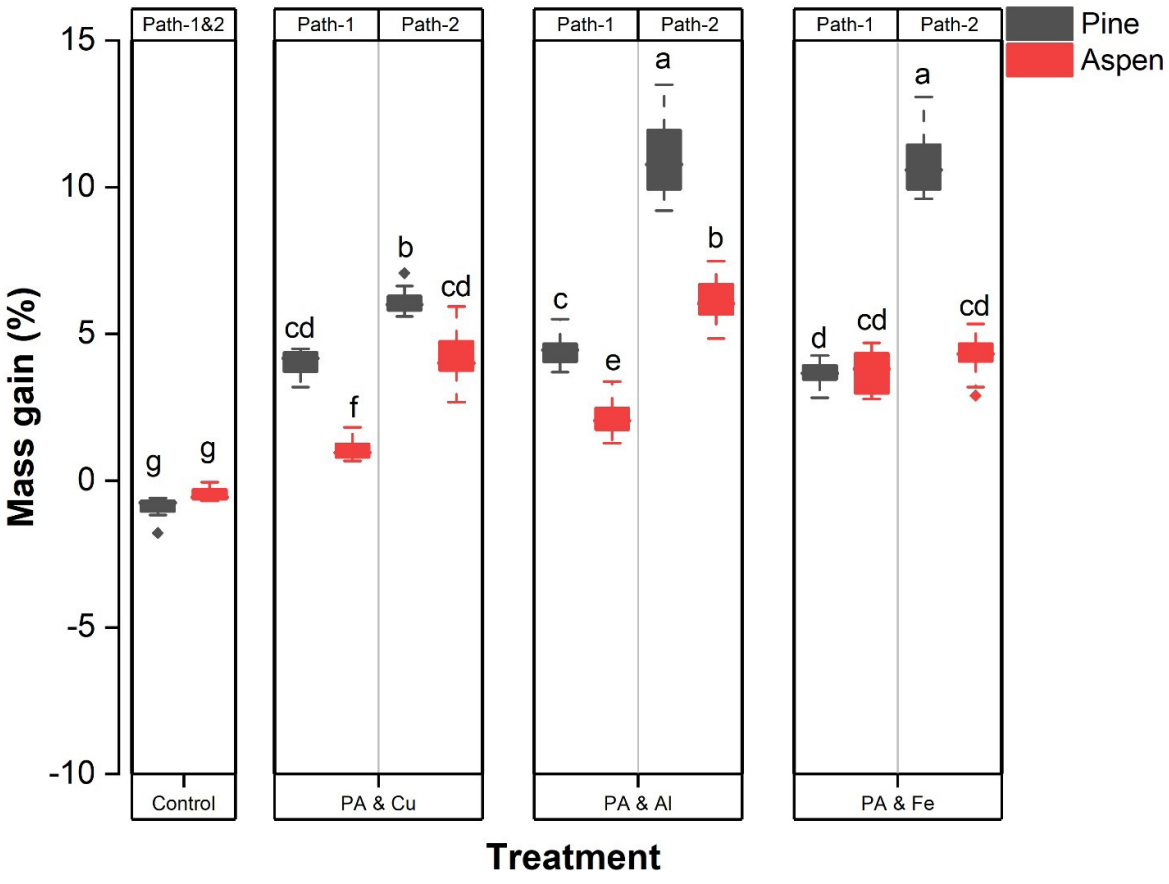

Figure S1. Mass gain of samples after treatment (n = 12).